IRWIN AND JOAN JACOBS
CENTER FOR COMMUNICATION AND INFORMATION TECHNOLOGIES

Gaussian beams scattered from different materials

Evyatar Hemo, Boris Spektor and Joseph Shamir

CCIT Report #753
December 2009

DEPARTMENT OF ELECTRICAL ENGINEERING
TECHNION - ISRAEL INSTITUTE OF TECHNOLOGY, HAIFA 32000, ISRAEL

CCIT REPORT #753 December 2009

Gaussian beams scattered from different materials

Evyatar Hemo[a] , Boris Spektor[a] and Joseph Shamir[a]

[a]Department of Electrical Engineering, Technion - Israel Institute of Technology, Haifa 32000, Israel

Investigating spherical nano-particles by illumination of Gaussian beam was studied. In order to simulate the scattering effect new software simulation based on the Bromwich formulation and the Mie theory was developed. The scattering simulation enables us to examine the scattered field affected by the particle size and material composition. Studying the scattered fields yielded sensors configuration which has the ability to differentiate between particles made of different materials.

1. Introduction

Advanced technology quite frequently encounters the need to analyze particles and surface features in the nanometer region. The most important aspects of interest are the size and material composition. Since we deal with dimensions under the wavelength of light, conventional imaging has significant limitations and different approaches must be investigated. In this work we assess the possibilities to extract information about the material composition of spherical nano-particles by observing the distribution of the scattered intensity when the investigated particles are illuminated by a focused Gaussian beam.

Table 1
Mainly studied materials and their refractive index.

Material	Refractive index
Glass	1.5
Gold	1.658+1.956i
Poly-Si	5.298+0.843i
GaAs	4.434+2.052i
Aluminum	0.503+4.923i
Diamond	2.458

In order to simulate the scattering effect a simulation software was developed based on the Bromwich formulation and the Mie theory to yield the beam shape coefficients (BSC). Analyzing the interaction of the beam with a sphere using the BSC method enables us to

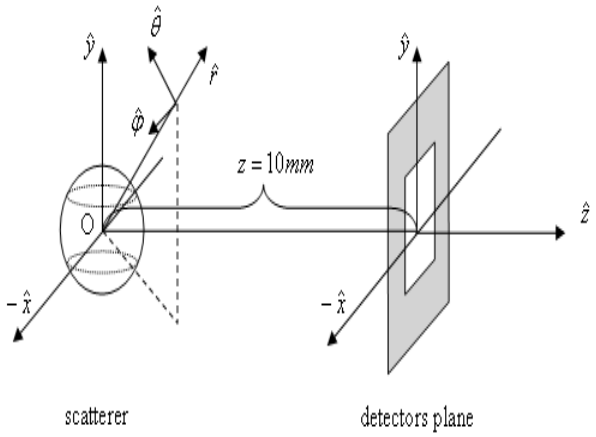

Figure 1. Coordinates system

get a different insight of the problem. Table 1 presents a list of material parameters that were studied as specific examples.

2. The simulation model

To simulate the scattering of a focused Gaussian beam on sub-wavelength spherical particles a new simulation software was developed based on the Mie theory. However, since the Mie theory was developed for plane wave illumination it must be generalized for illumination with more complex beam structures, such as Gaussian beams. Following the Bromwich formulation [1], [4] the electric and magnetic fields are detemined by the Bromwich potentials also known as the Hertz-Debye potentials. There are two potentials U_{TM} and U_{TE} which must fulfill the wave equation, which, in a spherical coordinate system, has the form,

$$\frac{\partial^2 U}{\partial r^2} + k^2 U + \frac{1}{r^2 \sin(\theta)} \frac{\partial}{\partial \theta} \left(\sin(\theta) \frac{\partial U}{\partial \theta} \right) + \frac{1}{r^2 \sin^2(\theta)} \frac{\partial^2 U}{\partial \varphi^2} = 0, \tag{1}$$

The TM and TE fields are defined with respect to the radial direction such that $H_r = 0$ and $E_r = 0$, respectively. They are calculated [5] from the solutions [3] of U_{TM} and U_{TE}. The origin of the coordinate system, O, is both at the center of the incident beam on the xy plane and the center of the scattering sphere. During the Bromwich formalism the scatterer center always remains the center of the coordinates system while the center of the beam can be relocated.

The radial component of the scattered electric field is given by

$$E_r = -kE_0 \sum_{n=1}^{\infty} \sum_{m=-n}^{+n} c_n g_{n,TM}^m a_n \left[\zeta_n'' (kr) + \zeta_n (kr)\right] P_n^{|m|} (\cos\theta) \exp(\imath m\varphi) \tag{2}$$

where k is the wave number, $k = M\frac{\omega}{c}$, ω is the angular frequency, c is the speed of light and M is the sphere's complex refractive index. The Bromwich beam coefficients of a plane wave, c_n, are given by

$$c_n = \frac{1}{\imath k} (-\imath)^n \frac{2n+1}{n(n+1)} . \tag{3}$$

and the structure of a beam is described by the beam shape coefficients, $g_{n,TM}^m$ and $g_{n,TE}^m$ that are 1 for a plane wave. The function, $\zeta_n (kr)$, is one of the Ricatti-Bessel functions defined by

$$\zeta_n (kr) = kr \cdot h_n^{(2)} (kr) = \left(\frac{\pi kr}{2}\right)^{\frac{1}{2}} H_{n+\frac{1}{2}}^{(2)} (kr) \tag{4}$$

where $H_n^{(2)} (kr)$ is a superposition of the Bessel and Neumann functions and is called the Hankel function of the second kind. The Hankel function has an important property of vanishing when $kr \to \infty$. $P_n^{|m|} (\cos\theta)$ are the well known associated Legendre polynomials and a_n are called Mie coefficients and will be explained further on.

The other components of the scattered electric field are

$$E_\theta = -\frac{E_0}{r} \sum_{n=1}^{\infty} \sum_{m=-n}^{+n} c_n \left[g_{n,TM}^m a_n \zeta_n' (kr) \tau_n^{|m|} (\cos\theta) + m g_{n,TE}^m b_n \zeta_n (kr) \Pi_n^{|m|} (\cos\theta)\right] \exp(\imath m\varphi) \tag{5}$$

$$E_\varphi = -\frac{\imath E_0}{r} \sum_{n=1}^{\infty} \sum_{m=-n}^{+n} c_n \left[m g_{n,TM}^m a_n \zeta_n' (kr) \Pi_n^{|m|} (\cos\theta) + g_{n,TE}^m b_n \zeta_n (kr) \tau_n^{|m|} (\cos\theta)\right] \exp(\imath m\varphi) \tag{6}$$

Where τ_n^m and Π_n^m are defined by

$$\tau_n^m (\cos\theta) = \frac{d}{d\theta} P_n^m (\cos\theta) \tag{7}$$

$$\Pi_n^m (\cos\theta) = \frac{P_n^m (\cos\theta)}{\sin\theta} \tag{8}$$

The scattering process is taken into account by the Mie coefficients a_n and b_n [2] that are expressed by

$$a_n = \frac{\Psi_n(x)\,\Psi_n'(y) - M\Psi_n'(x)\,\Psi_n(y)}{\zeta_n(x)\,\Psi_n'(y) - M\zeta_n'(x)\,\Psi_n(y)} \tag{9}$$

$$b_n = \frac{M\Psi_n(x)\,\Psi_n'(y) - \Psi_n'(x)\,\Psi_n(y)}{M\zeta_n(x)\,\Psi_n'(y) - \zeta_n'(x)\,\Psi_n(y)} \tag{10}$$

where $x = ka = \frac{2\pi a}{\lambda}$, $y = k_{sp}a$, a is the particle radius and k_{sp} is the wave number inside the sphere, therefore the refractive index is $M = \frac{k_{sp}}{k}$. The function $\Psi_n(kr)$ is one of the Ricatti-Bessel functions corresponding to the first order Bessel function. The full model will be rigorously described in Ref. [3].

It can be seen from Eqs. (2 - 6) that for a given incident illumination:

$$E_r^{incident} = \frac{E_0}{kr^2}\sum_{n=1}^{\infty}\sum_{m=-n}^{+n} c_n g_{n,TM}^m n(n+1)\,\Psi_n(kr)\,P_n^{|m|}(\cos\theta)\exp(\imath m\varphi) \tag{11}$$

$$H_r^{incident} = \frac{H_0}{kr^2}\sum_{n=1}^{\infty}\sum_{m=-n}^{+n} c_n g_{n,TE}^m n(n+1)\,\Psi_n(kr)\,P_n^{|m|}(\cos\theta)\exp(\imath m\varphi) \tag{12}$$

the scattered field is completely determined by the Mie coefficients that depend on the sphere's radius and refractive index. Therefore, the difference between the scattered fields of two different materials can be represented by these coefficients.

3. Shape of the scattered field distribution

As indicated above, for a particle positioned at a certain position within a given illuminating beam the Mie coefficients determine completely the scattered field components and thereby the shape of its distribution. While exploring the relations between the Mie coefficients and the scattered field distribution, several mathematical properties of these coefficients were studied. Studying the effects of the real part, the imaginary part, the absolute value and the phase of the Mie coefficients on the field distribution lead us to the conclusion that the most significant factor is the phase. It means that different scatterers that cause similar phases of the Mie coefficients will generate scattered field distribution of similar shape.

As a physical justification for this conclusion we may consider the Mie coefficients as spatial frequency coefficients since they originate from the decomposition process of the scattered field in the Legendre-Bessel basis. Therefore, the Mie coefficients have the meaning of frequency coefficients and it is a well known fact that the phase of the frequency coefficients have the strongest influence on the shape of an image.

To test the influence of the Mie coefficients on the shape of the scattered field distribution, dozens of scattering scenarios from both real and imaginary materials were

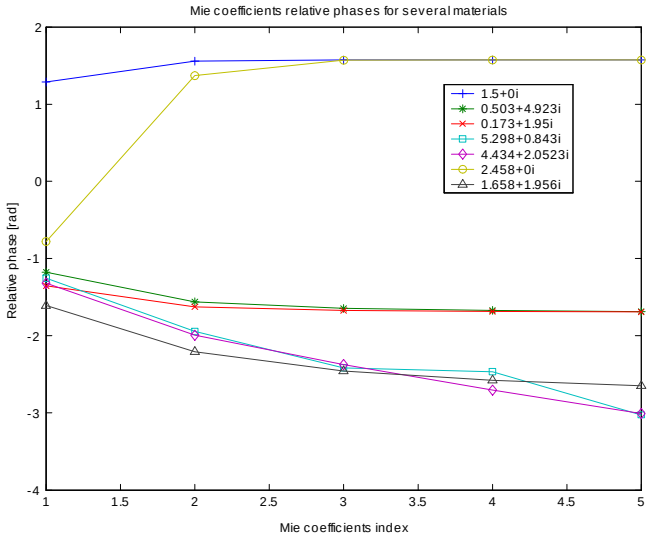

Figure 2. Mie coefficients relative phases for several materials

simulated. Imaginary materials with arbitrary refractive index were added to the simulations in order to enlarge the refractive index variety of the test. The phases of the first five Mie coefficients for the materials listed in the table above are shown in figure 2

and the respective scattered fields are presented in Fig. 3. For example, the coefficients for gold, poly-Si and GaAs have similar phases and they significantly differ from those for glass and diamond, in good correspondence with the shape of the scattered fields. Using this correspondence it is possible to predict which materials would cause scattered fields with similar shapes.

4. The effects of the NA on the scattered field distribution

In order to investigate the influence of the material on the scattered fields, several scenarios were simulated. These scenarios included X polarized Gaussian beams with different NA scattered from spheres of different materials and radius. Gaussian beams with $NA = 1, 0.5, 0.25$ (beam width of 0.25um, 0.5um and 1um respectively) scattered from a 100nm radius sphere were calculated 10mm from the sphere's center. The scattered intensities for $NA = 1$ are shown in figure 3.

As can be seen, different materials yield different scattered fields. Some of the fields have similar shapes while others are quite different. It is important to note that the sphere radius is small compared to the beam width. For a fixed sphere radius, as long as $\frac{a}{w_0} \lesssim 1$ where a is the sphere radius and w_0 is the beam width, the beam width has no influence on the scattered field distribution. The only thing that changes with the sphere radius is the intensity of the scattered field relative to the incident intensity. For larger beam width (lower NA), the energy hitting the sphere is smaller and so is the scattered field. However, when $\frac{a}{w_0} \gtrsim 1$ the scattered fields look completely different. For example, the

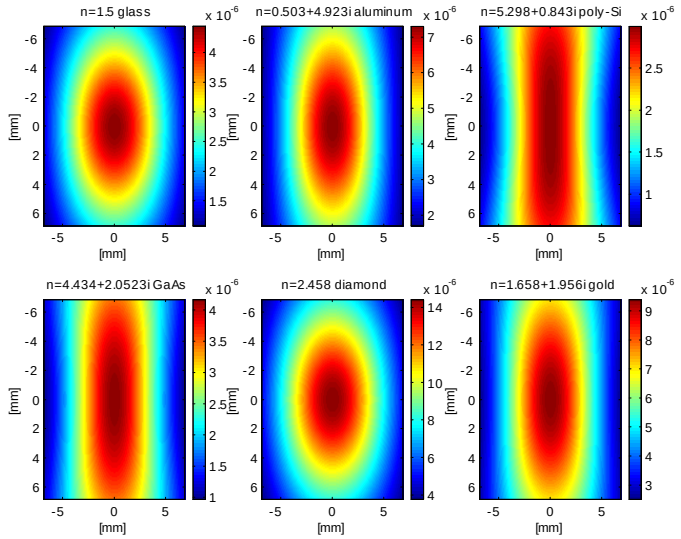

Figure 3. Scattered fields from several materials for a=100nm sphere

scattered field distributions of the same Gaussian beam from a 300nm spheres are quite different as can be seen from figure 4.

The results of the above simulations indicate that the material of particles can be classified by these measurements provided the condition $\frac{a}{w_0} \lesssim 1$ is maintained. Such a material classification can be done by calculating the eccentricity of the scattered field distribution. For example, within our set of materials, lower eccentricity values indicate glass or diamond while higher values are indication of semiconductor scatterers. In order to measure the eccentricity, the scattered fields were converted into binary images with threshold of 90% from the maximal energy. After retrieving the oval shapes (Fig. 5), the eccentricity parameter can be calculated as presented in Table 2 for various materials.

Table 2
Scattered fields eccentricity parameter.

Material	Eccentricity index	Material	Eccentricity index
Glass	0.718	Silver	0.821
Diamond	0.689	Poly-Si	0.972
GaN	0.657	GaAs	0.948
Aluminum	0.846	Germanium	0.945
Gold	0.899	Silicon	0.978
Copper	0.88	SiO	0.927

Particles made of materials such as Si, Ge and GaAs which are commonly used in the

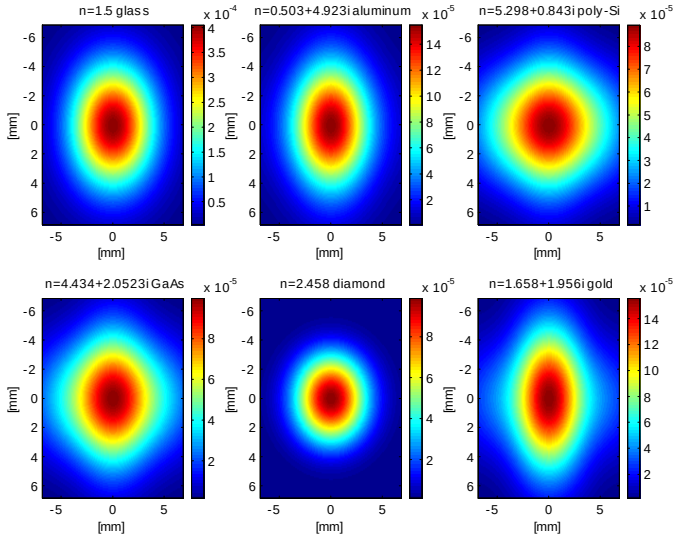

Figure 4. Scattered fields from several materials for a=300nm sphere

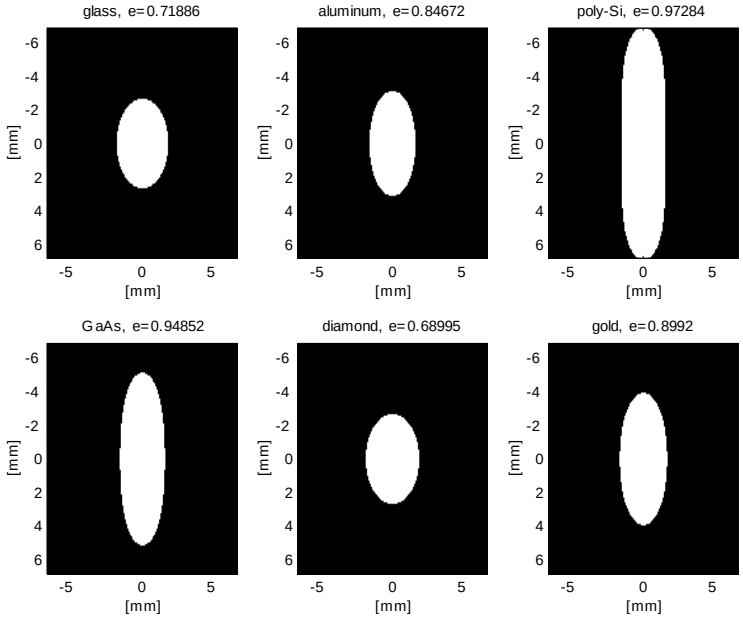

Figure 5. Binary images of the scattered fields

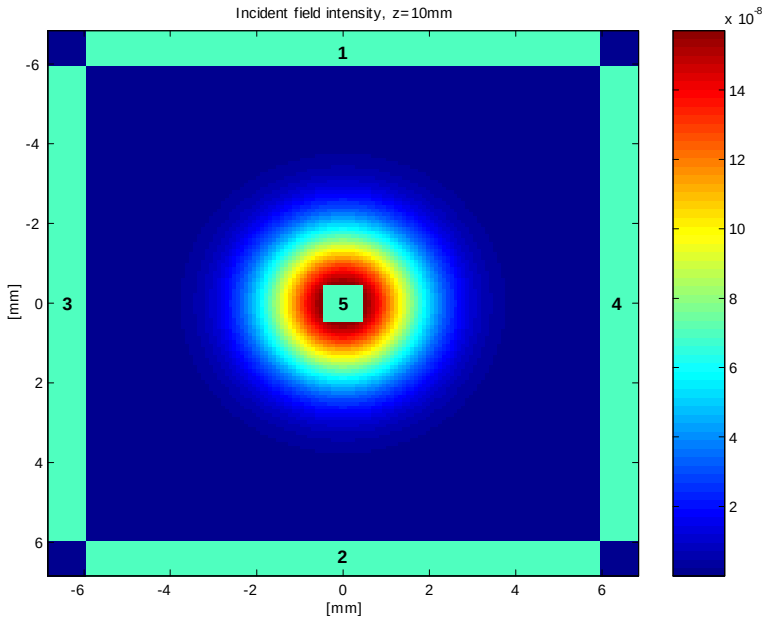

Figure 6. Detectors configuration

semiconductor industry have high eccentricity values (> 0.94) while glass and diamond particles have small values (< 0.72). Metals have intermediate values, closer to the semiconductors.

5. Material classification

To classify the material composition of nano-particles it is suggested to use the eccentricity property of the scattered fields. Combining the fact that the Gaussian beam is spatially finite (as opposed to a plane wave, for example) it is possible to design a special detector architecture which enables us to classify different materials. The scattered intensity is low relative to the incident intensity therefore the total measured field will not have distinguishable eccentricity values at its center. However, by setting the detectors far enough from the incident beam's maximal intensity region but adequately close to still have significant values of the scattered field, it is possible to estimate the material composition of sub-wavelength particles. The detector configuration shown in Fig. 6 is composed of two pairs of parallel rectangular detectors. The first pair, perpendicular to the y axis, is located 6.8[mm] from the center of the beam and the second pair is located at the same distance perpendicular to the x axis. The size of each of the four detectors is 0.9x11.8[mm].

For the proposed estimation we measure the total power incident on the first parallel pair and divide it with the power measured over the second parallel pair. Calculating this power ratio enables us to calculate indirectly the eccentricity effect of the scattered fields. To eliminate the influence of the absolute power of the scattered fields this ratio is

multiplied by a normalization factor. The normalization factor is the ratio between the maximal intensity of the total field and the maximal intensity of the incident field (the total field in case that there is no scatterer). In order to measure the normalization coefficient a fifth 0.9x0.9[mm] detector was added at the center of the beam. The normalized intensity ratio (NIR) is thereby given by

$$NIR = \left(\frac{P(d_1) + P(d_2)}{P(d_3) + P(d_4)} \right) \cdot \frac{P(d_5)}{P(d_5)\,|_{no\ scatterer}} \tag{13}$$

where $P(d_i)$ is total power measured by the detectors:

$$P(d_i) = \int_{d_i} \left(|E_x|^2 + |E_y|^2 \right) ds$$

where E is the total field calculated at the detector plane and d_i is the relevant detector. The NIR measurement indicates the eccentricity of the scattered fields and thereby the scatterer material. It is important to note that the above sensor configuration is based on the assumption that the incident Gaussian beam is x polarized. As a consequence the semi-major axis of the elliptic shaped of the scattered intensity is y. This asymmetry was taken into account when the power received by the detectors perpendicular to the y axis was placed in the numerator of the NIR expression. Several NIR values are listed in the next table.

Table 3
NIR values.

Material	NIR	Material	NIR
Glass	1.43	Silver	1.66
Diamond	1.18	Poly-Si	2.37
GaN	1.15	GaAs	2.10
Aluminum	1.70	Germanium	2.10
Gold	1.77	Silicon	2.94
Copper	1.76	SiO	1.90

As can be seen, it is possible to identify families of materials such as glass, diamond and GaN having low NIR values ($NIR \lesssim 1.5$), metals having medium NIR values $1.6 \lesssim NIR \lesssim 1.8$ and the semiconductors having high NIR values $NIR > 1.9$.

6. Conclusions

Using new scattering simulation software it was possible to investigate the influence of the particle material and size on the shape of the scattered field distribution. It was

found that while the condition $\frac{a}{w_0} \lesssim 1$ is maintained it is possible to sort scatterers into different families of materials. The material classification is based on the eccentricity of the scattered field distribution, which has a strong dependence on the relative phases of the Mie coefficients. Exploiting these results it is possible to predict which materials will cause similar scattered fields just by calculating the Mie coefficients of a scatterer without simulating the scattered field itself. Finally, a detector architecture was offered to measure the eccentricity property of the scattered fields for the classification of the material composition of scattering nano-particles.

REFERENCES

1. G. Gouesbet, B. Maheu and G. Grehan, "Light scattering from a sphere arbitrarly located in a Gaussian beam, using a Bormwich formulation" J. Opt. Soc. Am. A, Vol. 5, No.9, p.1427 (1988)
2. H.C. van de Hulst, *Light Scattering by small particles,* Dover Publications, Inc. New York, 1981
3. E. Hemo, B. Spektor and J. Shamir "Singular beams interaction with subwavelength particles" in preparation.
4. Milton Kerker, *The Scattering Of Light*, Academic Press, New York and London, 1969
5. Cheng-Wei Qiu and Le-Wei Li, "Electromagnetic scattering by 3-D general anisotropic objects: a Hertz- Debye potential formulation", in Proc. of 2005 IEEE AP-S International Symposium And USNC/URSI National Radio Science Meeting, Washington D.C., USA, July 3-8, 2005.